Chinese Journal of
POLYMER SCIENCE

ARTICLE

https://doi.org/10.1007/s10118-021-2550-y
Chinese J. Polym. Sci. **2021**, *39*, 887–895

Influence of Liquid Isoprene Rubber on Strain Softening of Carbon Black Filled Isoprene Rubber Nanocomposites

Feng-Yi Hou, Yi-Hu Song*, and Qiang Zheng

MOE Key Laboratory of Macromolecular Synthesis and Functionalization, Department of Polymer Science and Engineering, Zhejiang University, Hangzhou 310027, China

Electronic Supplementary Information

Abstract The reinforcement of rubbers by nanoparticles is always accompanied with enhanced dissipation of mechanical energy upon large deformations. Methods for solving the contradiction between improving reinforcement and reducing energy dissipation for rubber nanocomposites have not been well developed. Herein carbon black (CB) filled isoprene rubber (IR)/liquid isoprene rubber (LR) blend nanocomposites with similar crosslink density (ν_e) are prepared and influence of LR on the strain softening behaviors including Payne effect under large amplitude shear deformation and Mullins effect under cyclic uniaxial deformation is investigated. The introduction of LR could improve the frequency sensitivity of loss modulus and reduce critical strain amplitude for Payne effect and loss modulus at the low amplitudes. Meanwhile, tuning ν_e and LR content allows reducing mechanical hysteresis in Mullins effect without significant impact on the mechanical performances. The investigation is illuminating for manufacturing nanocomposite vulcanizates with balanced mechanical hysteresis and reinforcement effect.

Keywords Rubber nanocomposites; Stress softening; Mechanical hysteresis; Liquid rubber

Citation: Hou, F. Y.; Song, Y. H.; Zheng, Q. Influence of liquid isoprene rubber on strain softening of carbon black filled isoprene rubber nanocomposites. *Chinese J. Polym. Sci.* **2021**, *39*, 887–895.

INTRODUCTION

Nanoparticles are widely used for reinforcing rubber materials, which is ascribed to the hydrodynamic effect,[1–3] filler-rubber interfacial interaction[4] and filler aggregation and percolation.[5–8] Apart from the reinforcement effect, the addition of nanofillers also promotes strain softening including Payne effect appeared in large-amplitude oscillational shear[9,10] and Mullins effect in cyclic tensile deformation.[11] The softening has been attributed to deagglomeration of filler clusters,[12–15] slippage and/or desorption of chains from filler surface,[16,17] and viscoelastic effects rooted in the rubbery matrix.[18–22] The ambiguity and misunderstanding of the strain softening make it difficult to optimize the reinforcement and dissipation behaviors of rubber nanocomposites.

In practice, the rubber matrix in the nanocomposites is commonly crosslinked. However, an absolute control on the crosslinking reaction is difficult and the rubber networks are rich in defects including free and dangling chains. The network defects influence the network dynamics,[23,24] viscoelasticity[25–28] and damping behavior.[29–31] The use of high amounts of fillers to meet the engineering applications would strongly interfere with the crosslinking reaction by adsorption of not only rubber chains but also curing and processing agents,[32–34] which further brings difficulty in balancing the reinforcement and dissipation behaviors.

There are no attempts to lessen dissipation accompanying the Mullins effect in rubber nanocomposites. Herein liquid isoprene rubber (LR) is used to mediate the crosslinking network of carbon black (CB) filled isoprene rubber (IR) vulcanizates. The addition of LR could reduce the mechanical hysteresis without significant impact on the mechanical performances. LR participates in the network formation and is hard to migrates from the nanocomposites,[35–39] providing a promising method for preparing rubber nanocomposites with low mechanical hysteresis and high reinforcement effect.

EXPERIMENTAL

Materials

Liquid isoprene rubber (LR, trademark LIR-30) with weight-averaged molecular weight of 30 kg/mol, polydispersity of 1.10, and glass transition temperature (T_g) of –65.3 °C (Fig. S1a in the electronic supplementary information, ESI) was purchased from Kuraray Co., Ltd., Japan. Isoprene rubber (IR, trademark IR2200) with more than 98% *cis*-1,4 structure, weight-averaged molecular weight of 1220 kg/mol and polydispersity of 2.0 was produced by Zeon Chem., Japan. Carbon black (N330) with particle size about 30 nm was purchased from Longxin Chem. Stock Co., Ltd., China. Sulfur and antioxidant of *N*-(1,3-

* Corresponding author, E-mail: s_yh0411@zju.edu.cn

Received December 3, 2020; Accepted January 11, 2021; Published online April 14, 2021

dimethylbutyl)-*N*'-phenyl-*p*-phenylenediamine (6PPD) were obtained from Kunshan Anzhe Chem. Stock Co., Ltd., China and Zhejiang Yongjia Chem. Plant, China, respectively. Activator zinc oxide (ZnO) and stearic acid were purchased from Shanghai Macklin Biochem. Co., Ltd., China and Tokyo Chem. Co., Ltd., Japan, respectively. Accelerator *N*-cyclohexyl-2-benzothiazolesulfenamide (CZ) was purchased from Aladdin, China.

Sample Preparation

Table 1 lists formulations of the nanocomposites. The IR gum was first mixed with 1 phr (parts per hundred parts of rubber) 6PPD, 2.5 phr steric acid and 4 phr ZnO (not included in Table 1) at 100 °C and 40 r/min for 10 min *via* an internal mixer (XSS-300, Kechuang Rubber Plastic Mechan. Equipment Co., Ltd., China). After adding LR and CB, the compounds were mixed at 100 °C and 40 r/min for 20 min. Finally, CZ and sulfur were added in the compounds at 80 °C and 30 r/min for 10 min.

Table 1 Formulations of the compounds and their curing time for preparation of the vulcanizates. [a]

Sample	IR	LIR-30	CB	CZ	S	Curing time (min)
IR/0LR-20CB	100	–	20	0.55	0.55	45
IR/0LR-40CB	100	–	40	0.55	0.55	43
IR/0LR-60CB	100	–	60	0.55	0.55	50
IR/0.4LR-20CB	71.4	28.6	20	0.95	0.95	43
IR/0.4LR-40CB	71.4	28.6	40	1.00	1.00	45
IR/0.4LR-60CB	71.4	28.6	60	1.05	1.05	37

[a] Amounts of raw materials and chemicals are presented in phr.

The carbon black gel (CBG) in the highly filled compounds was obtained *via* extraction experiment. The uncured compounds were extracted by toluene for 10 days and by renewing toluene every 2 days. At low CB contents, intact CBG could not be obtained due to the leakage of CB particles into solvent and the dissolution of the rubber.

To prepare nanocomposite vulcanizates, the compounds were compressed into sheets of 2 mm in thickness at 140 °C by a vulcanizer (XL-25, Huzhou Xinli Rubber Machinery Co., Ltd., China). The curing time (Table 1) was prescribed as the optimal vulcanization time determined from dynamic vulcanization curves.

The compounds, CBG and vulcanizates were named as IR/*i*LR-*j*CB-C, IR/*i*LR-*j*CB-CBG and IR/*i*LR-*j*CB-V_z, respectively. Here the letters "*i*" and "*j*" represent the ratio of LR to IR and the content of CB in phr, respectively, and "*z*" stands for crosslinking density (ν_e) of the matrix in mol/m^3. For better comparison, ν_e was manipulated to be similar for vulcanizates with the same CB contents. For manipulating the mechanical hysteresis in cyclic deformations, vulcanizates with higher ν_e or LR to IR ratio were also prepared (Table S1 in ESI) by curing for 23, 21 and 32 min, respectively.

Characterizations

The dispersion of CB in the matrix was observed by transmission electron microscope (TEM, JEM-1200EX, JEOL, Japan) at an accelerating voltage of 300 kV. The samples were obtained by ultramicrotomy.

Toluene was used to swell the vulcanizates at room temperature for 48 h. Flory-Rehner equation $\nu_e = -[\ln(1 - V_r) + V_r + \chi V_r^2]/[V_0(V_r^{1/3} - V_r^{1/2})]$ was utilized to calculate ν_e. Here V_0, V_r and χ are the molar volume of solvent (105.7 ml/mol), volume fraction of rubber in swollen samples and polymer-solvent interaction parameter estimated by $0.427+0.112V_r^2$, respectively.[40]

The weight percentage of bound rubber in the compounds and CBG was determined by weighting method. Thermogravimetric analysis (TGA, Q1000, TA Instruments, USA) was also applied to estimate the bound rubber content in CBG. Samples were heated from room temperature to 800 °C at a rate of 10 °C/min in nitrogen atmosphere.

Modulated differential scanning calorimetry (MDSC, Discovery 25, TA Instruments, USA) was used to test increment of heat capacity (ΔC_p) of the nanocomposites across glass transition of the matrix. The samples after equilibrium at −85 °C for 5 min were heated to −45 °C at a rate of 1 °C/min with modulated signal time of 2 min and amplitude of ±1 °C. The bound layer content was calculated according to $1-\Delta C_p/[(1-w)\Delta C_{p,IR}]$. Here w is the CB weight fraction in the nanocomposites and $\Delta C_{p,IR}$ is the increment of heat capacity of the matrix during glass transition.

Molecular weight and polydispersity of the sol fractions extracted from the compounds were measured by a gel permeation chromatography (GPC, Water 2690, Water Co., USA) at 40 °C and flow rate of 1 mm/min. Tetrahydrofuran was used as solvent.

The rheological behaviors of the compounds and vulcanizates were measured by a rheometer (ARES-G2, TA Instruments, USA) at 60 °C. The linear rheological responses were measured in the frequency (ω) range from 100 rad/s to 0.025 rad/s at strain amplitude (γ) of 0.1%. The strain amplitude sweep experiment was conducted in the γ range from 0.01% to 80% at 1 rad/s.

Dumbbell shaped samples of 4 mm in width, 2 mm in thickness and 25 mm in length of working section were used for tensile test using a tester (Suns Zongheng Technol. Co., Ltd., Shenzhen, China) at room temperature and at a crosshead velocity of 500 mm/min. The cyclic loading-unloading uniaxial tensile deformations with increasing maximum prestrains at each cycle were performed at step strain of 100% at crosshead velocity of 50 mm/min. The area of hysteresis loop in one loading-unloading cycle and that under the loading stress curve are defined as E_h and E respectively, and E_h/E is used to describe the ratio of energy dissipation in each cycle.

RESULTS AND DISCUSSION

Microstructure and Interfacial Interaction of the Nanocomposites

Fig. 1 shows TEM images of the vulcanizates. The CB nanoparticles are distributed rather homogeneously in the matrix. The degree of CB agglomeration increases at high CB contents while the composition of the matrix does not influence the CB dispersity significantly. The presence of LR has no influence on the distribution of other additives such as ZnO activator (Fig. S2 in ESI).

The adsorption of chains on the surface of CB nanocomposites leads to the formation of bound rubber depending on chains size[41,42] and filler content.[43,44] The bound rubber and CB constitute CBG in which a small fraction of strongly immobilized chains forms a thin glassy layer surrounding CB

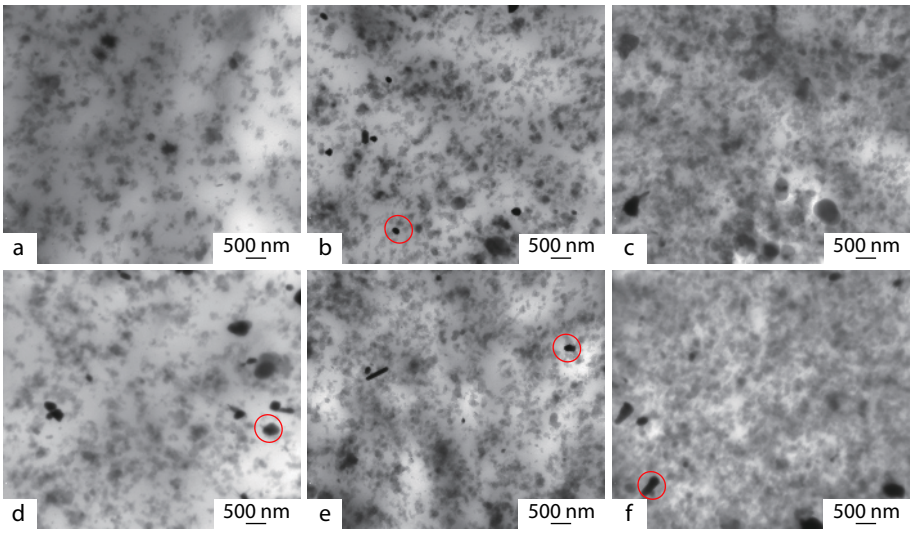

Fig. 1 TEM images of IR/0LR-20CB-$V_{64.3}$ (a), IR/0LR-40CB-$V_{76.5}$ (b), IR/0LR-60CB-$V_{110.4}$ (c), IR/0.4LR-20CB-$V_{70.1}$ (d), IR/0.4LR-40CB-$V_{79.3}$ (e), and IR/0.4LR-60CB-$V_{111.8}$ (f). The red circles indicate ZnO particles.

Table 2 T_g and composition of CBG.

CBG	T_g (°C)	$\Delta C_p/(1-w)$ [J/(g·°C)]	Glassy layer content (%)	Rubber content (%)	
				Weighting	TGA
IR/0LR-40CB-CBG	−67.4	0.362	2.1	31.3	27.2
IR/0.4LR-40CB-CBG	−67.4	0.364	7.8	29.5	25.8
IR/0LR-60CB-CBG	−67.2	0.371	ND [a]	33.0	30.4
IR/0.4LR-60CB-CBG	−67.3	0.362	8.3	30.4	26.4

[a] Not detectable.

nanoparticle. As shown in Table 2, T_g of bound rubber in the CBG is the same as that of the matrix (Fig. S1 in ESI). The CBG contains about 30% bound rubber (Table 2 and Fig. S3 in ESI), being independent of filler content and rubber composition. Normalized increment of heat capacity, $\Delta C_p/(1-w)$, is about 0.365 J/(g·°C), which corresponds to glassy layer content less than 10 % (Table 2), indicating a slight degree of chain immobilization.

The sol fraction extracted from the IR/0.4LR-20CB-C, IR/0.4LR-40CB-C and IR/0.4LR-60CB-C compounds demonstrates bimodal distribution (Fig. S4 in ESI), from which the content of the low molecular weight fraction is determined as 46.3%, 32.6% and 38.5%, respectively, being higher than that of LR in the matrix (28.6%) of the compounds. It indicates that long chains participate in the bound rubber formation preferentially.

The introduction of LR leads to the formation of more chain ends and more sulfur is required to maintain v_e the same as that of the IR vulcanizates at given CB contents (Table 1 and Table 3). The presence of LR raises the sol content slightly (Table 3) while most of chains are connected to the crosslinking network. Although v_e and CB contents are different, T_g and $\Delta C_p/(1-w)$ of the vulcanizates are similar (Table 3; DSC curve referencing to Fig. S1 in ESI). Thus, the influences of T_g and glassy chains on the rheological and deformation behaviors will not be considered further.

Rheological Behaviors of the Nanocomposites

The introduction of CB significantly influences the linear rheological behavior of the uncured compounds (Fig. 2). For the

Table 3 Parameters of the vulcanizates.

Sample	v_e (mol/m^3)	Sol content (wt%)	T_g (°C)	$\Delta C_p/(1-w)$ [J/(g·°C)]
IR/0LR-20CB-$V_{64.3}$	64.3±1.4	2.39	−66.2	0.412
IR/0LR -40CB-$V_{76.5}$	76.5±1.6	2.79	−66.2	0.426
IR/0LR -60CB-$V_{110.4}$	110.4±4.7	2.64	−66.3	0.429
IR/0.4LR -20CB-$V_{70.1}$	70.1±3.3	6.22	−65.1	0.429
IR/0.4LR-40CB-$V_{79.3}$	79.3±4.1	6.87	−65.4	0.432
IR/0.4LR -60CB-$V_{111.8}$	111.8±0.1	7.20	−65.3	0.420

compounds with IR or IR/0.4LR matrix, the frequency (ω)-dependences of storage modulus (G') and loss modulus (G'') weaken gradually with increasing CB content. The presence of LR lowers both G' and G''. The variations of linear rheological behavior could be ascribed to the strain amplification effect induced by CB and the bound rubber formation at high CB contents. LR could reduce the bound rubber content slightly. In the IR/0LR-40CB-C, IR/0.4LR-40CB-C, IR/0LR-60CB-C and IR/0.4LR-60CB-C compounds, the bound rubber contents are 18.3%, 16.7%, 29.5% and 26.2%, respectively. However, both the segmental dynamics (Table 2) and bound rubber content are not determinative influencing factors of the rheological behaviors.

Fig. 3 shows nonlinear Payne effect of IR/0LR-*j*CB-C and IR/0.4LR-*j*CB-C compounds. Both G' and G'' are invariant in the low γ region (the values being denoted as G'_0 and G''_0, respectively) while they decay markedly at γ above a critical amplitude (γ_c). The additions of CB and LR lower γ_c. Fig. 4

https://doi.org/10.1007/s10118-021-2550-y

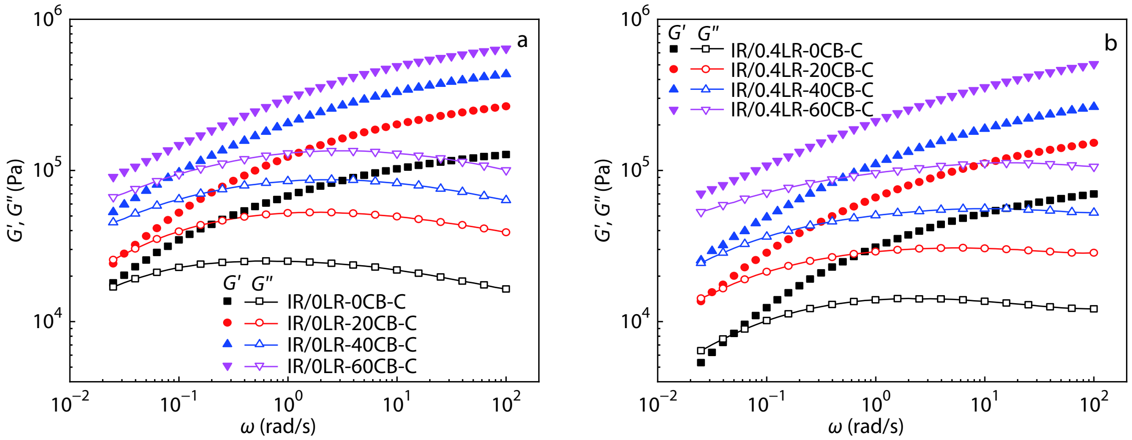

Fig. 2 G' (solid symbols) and G'' (lines and hollow symbols) as function of ω for IR/0LR-*j*CB-C (a) and IR/0.4LR-*j*CB-C compounds (b).

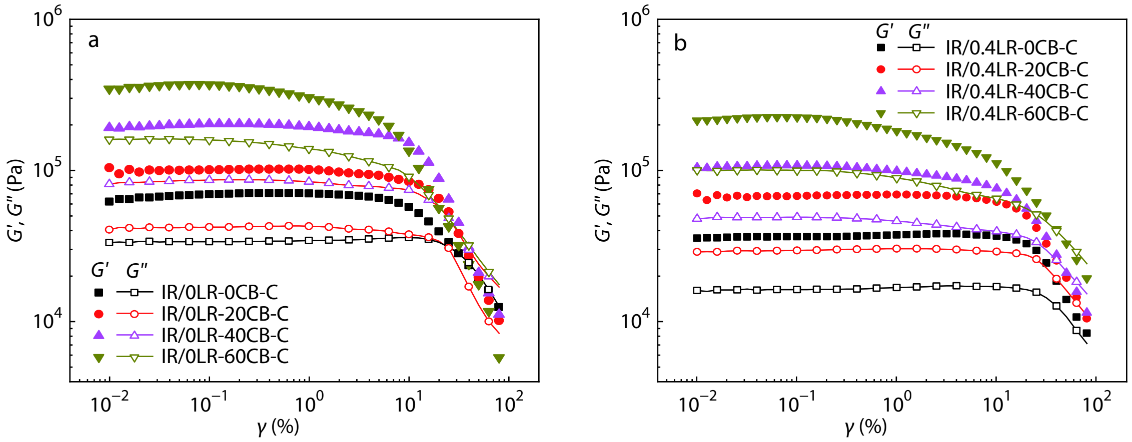

Fig. 3 G' (solid symbols) and G'' (lines and hollow symbols) as function of γ for IR/0LR-*j*CB-C (a) and IR/0.4LR-*j*CB-C compounds (b).

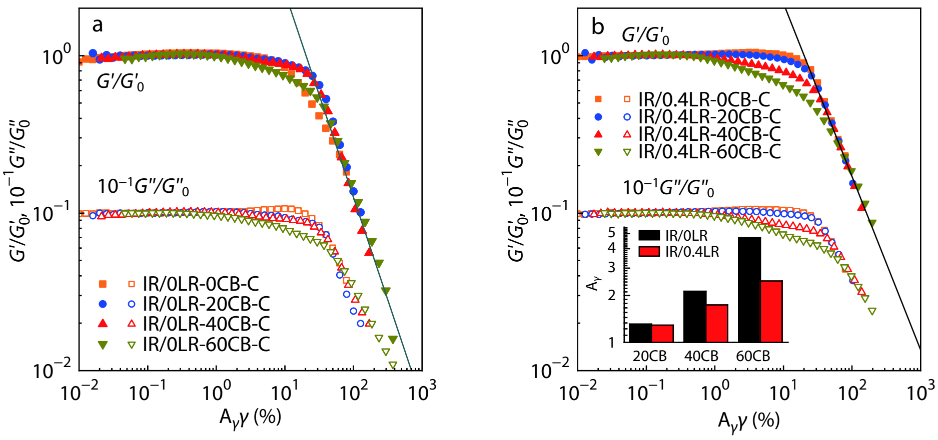

Fig. 4 Normalized plots of G'/G'_0 (solid symbols) and G''/G''_0 (hollow symbols) as a function of $A_\gamma\gamma$ for IR/0LR-*j*CB-C (a) and IR/0.4LR-*j*CB-C compounds (b). Inset in (b) shows strain amplitude factor A_γ. The lines in (a) and (b) are drawn according to $\gamma^{-1.3}$ and $\gamma^{-1.1}$, respectively.

shows the normalized plots of G'/G'_0 and G''/G''_0 as a function of $A_\gamma\gamma$. Here A_γ is strain amplification factor that is determined as horizontal shifting factor for creating master curves with reference to the nonlinear rheological curves of the matrix. It can be observed that A_γ increases with filler content and is smaller in the IR/0.4LR compounds than in the IR/0LR ones (inset in Fig. 4). It means that the occurrence of Payne effect may be influenced by the molecular weight distribution of the matrix.[45,46] It should be noted that, at 40–60 phr CB, the compounds demonstrate a two-step softening and the first

one occurred at γ=1%–10% is more obvious for the IR/0.4LR compounds. The first softening is possibly related to breakup of some filler structures.[47]

LR influences the linear and nonlinear rheological responses of the nanocomposites vulcanizates. Fig. 5 illustrates G' and G'' as a function of ω. The ω-sensitivities of G' and G'' are much weaker than those of the compounds. The presence of LR lowers G' on the one hand and improves the ω-sensitivity of G'' on the other hand. Fig. 6 shows Payne effect of the vulcanizates. The G'' curves demonstrate weak strain overshoot (type III behavior), which differs from the sustain softening (type I behavior) of the compounds (Fig. 3). With increasing filler content, γ_c becomes smaller and the weak strain overshoot becomes weaker.

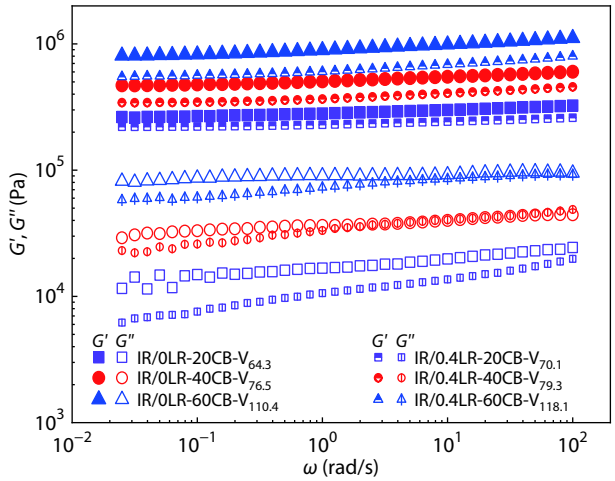

Fig. 5 G' and G'' as function of ω for vulcanizates.

Fig. 7 shows normalized plots of G'/G'_0 and G''/G''_0 as a function of $A_\gamma\gamma$. The superposition is well for G'/G'_0 while fails for G''/G''_0, exhibiting weak strain overshoot. The normalized plots of G'/G'_0 of the vulcanizates even overlap that of the uncured gum, suggesting that the crosslinking and filling do not alter the major mechanisms of the G' decay accompanying the Payne effect. However, A_γ in IR/0.4LR-*j*CB vulcanizates is higher than that in the IR/0LR-*j*CB vulcanizates at given CB contents, which is in contradiction with the compounds (Fig. 4). In the nonlinear region, G' varies as γ^{-x} with x=1.1 and x=1.3 for the IR/0LR-*j*CB and IR/0.4LR-*j*CB vulcanizates, respectively. The scaling exponents are close to those in the uncured compounds (Fig. 4) and in silica filled polydimethylsiloxane vulcanizates,[48] being in agreement with the predictions (x=4/3[49] and x=1[50]) of Rouse model, revealing the importance of Rouse dynamics to the occurrence of Payne effect.

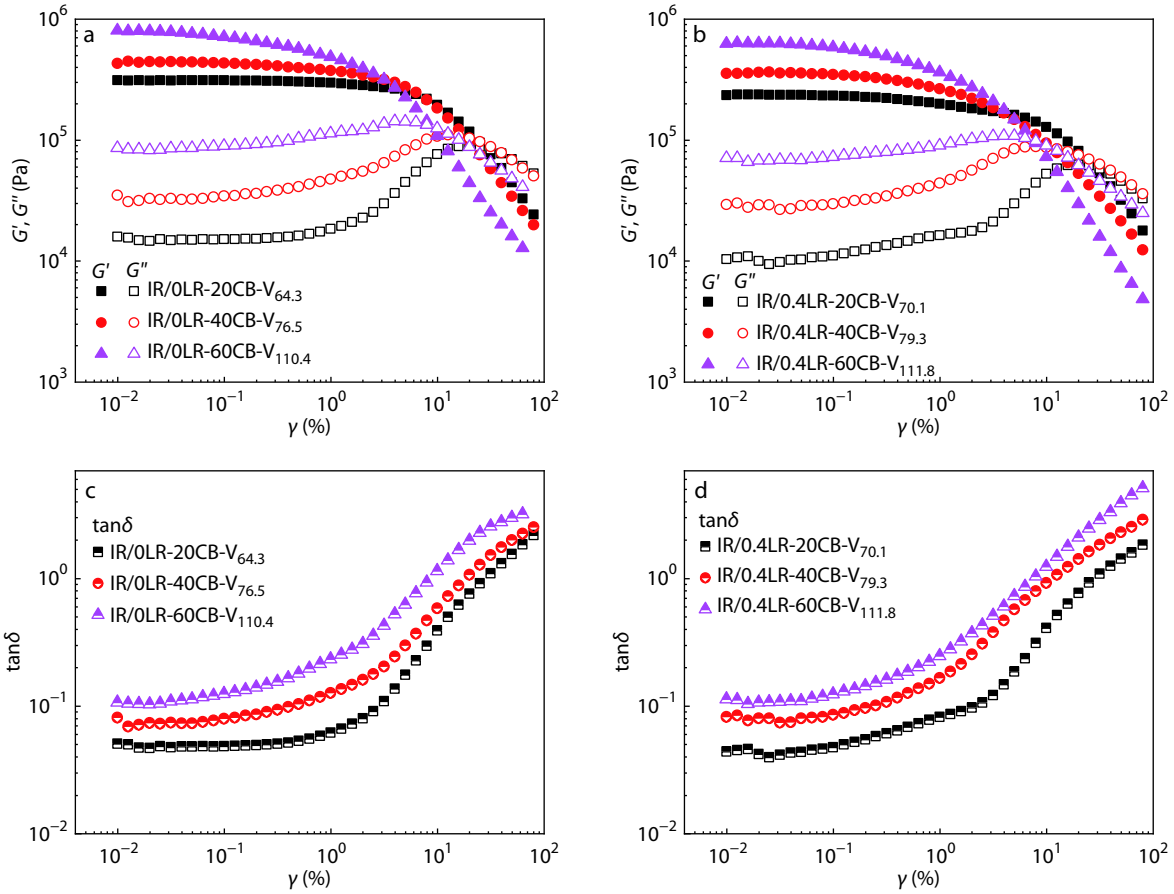

Fig. 6 G' (solid symbols, a and b), G'' (hollow symbols, a and b) and tanδ (half-filled symbols, c and d) as a function of γ for IR/0LR-*j*CB-V$_z$ (a and c) and cured IR/0.4LR-*j*CB-V$_z$ vulcanizates (b and d).

https://doi.org/10.1007/s10118-021-2550-y

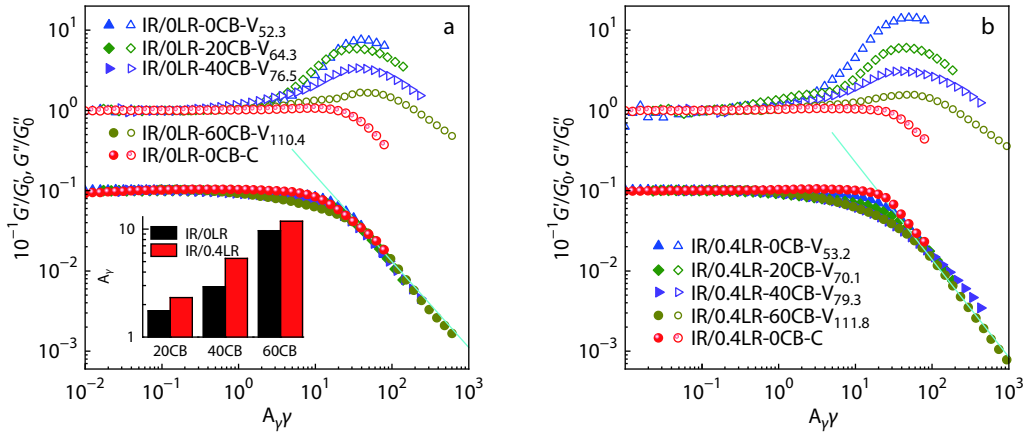

Fig. 7 Normalized plots of G'/G'_0 (solid symbols) and G''/G''_0 (hollow symbols) as a function of $A_\gamma\gamma$ for IR/0LR-*j*CB-V$_z$ (a) and IR/0.4LR-*j*CB-V$_z$ vulcanizates (b). Inset in (a) shows strain amplitude factor A_γ of the vulcanizates. The data of uncured gums (IR/0LR-0CB-C and IR/0.4LR-0CB-C) are shown for comparison. The lines in (a) and (b) are drawn according to $\gamma^{-1.1}$ and $\gamma^{-1.3}$, respectively.

Uniaxial Tensile Deformation of Vulcanizates

Fig. 8 shows stress-strain curves of vulcanizates. At given CB contents and similar v_e, the presence of LR dose not impair the mechanical performances. The vulcanizates during cyclic deformation demonstrate Mullins effect characterized by mechanical hysteresis and stress softening (Fig. 9). At given strains, the unloading stresses of the IR/0.4LR-*j*CB-V$_z$ vulcanizates are higher than those of the IR/0LR-*j*CB-V$_z$ ones. The differences become smaller with increasing CB content. Both E and E_h increase with increasing CB content and prestrain whereas the existence of LR reduces E_h and relative hysteresis energy E_h/E (Fig. 10). In filled vulcanizates, the physical interactions would be interrupted during loading and reform partially during the unloading process, which contributes to the Mullins effect. The introduction of LR in the nanocomposites has no influence on the filler-rubber interactions as evidenced by the small amount of glassy content and the similar bound rubber content (Table 2). Furthermore, LR has no influence on the filler dispersion (Fig. 1). It means that the reductions in E_h and E_h/E are not determined by the variations in filler structure and interfacial interaction. Such result highlights the vital role of rubber network structures including entanglement density, defect chains and v_e on the stress softening, which is in contradiction with previous arguments that the mechanical hysteresis mainly involves in the destruction of filler structure and interfacial interactions.[16,51–56] In the nanocomposites, LR participates in the crosslinking network formation, which is expected to generate a great number of dangling chains along with the production of a slightly increased sol fraction (Table 3). The LR chains connecting the CB nanoparticle and the rubber network should recoil prior to the long IR chains during the unloading process, promoting the hysteretic recovery of the deformation and lowering E_h/E.

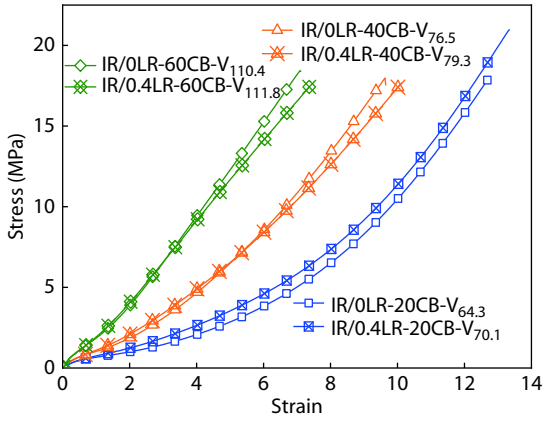

Fig. 8 Stress-strain curve for vulcanizates.

Since the mechanical hysteresis is mainly related to rubber network, it could be tuned *via* regulating the LR content and v_e at given CB loadings (Table S1 in ESI). At similar v_e for the 60 phr CB filled vulcanizates, the introduction of LR has little effect on tensile strength and strain at break (Fig. S5 in ESI). At v_e≈200 mol/m^3 and 60 phr CB, LR does not influence the loading stress while improves the unloading stress, promotes the hysteretic recovery and largely reduces E_h/E at high prestrains (Figs. S6 and S7 in ESI). At v_e≈116 mol/m^3 and 60 phr CB, E_h/E at high prestrains decreases markedly with the increasing LR to IR ratio (Fig. 10c and Fig. S7c in ESI). Thus, the use of LR in combination with filling and crosslinking provides a potential way to prepare rubber nanocomposites with balanced mechanical performance and energy dissipation.

It is shown that the introduction of LR brings a promising balance between the mechanical hysteresis and reinforcement for the IR nanocomposite vulcanizates. The introduction of LR would bring complicated variations in molecular structure of the crosslinking network. It introduces structural heterogeneities associated with generation of chain branches and dangling ends that would restrain the molecular alignment along the stretch axis. The local crosslinking density and network defects in the vulcanized matrix should possibly contribute to the reduced energy dissipation in cyclic deformation. It is expected that the effects of LR should be dependent on the weight ratio of LR to IR, the molecular weight and its distribution of LR, and the competitive interactions of CB, sulfur and the other additives with LR and IR, which should be

https://doi.org/10.1007/s10118-021-2550-y

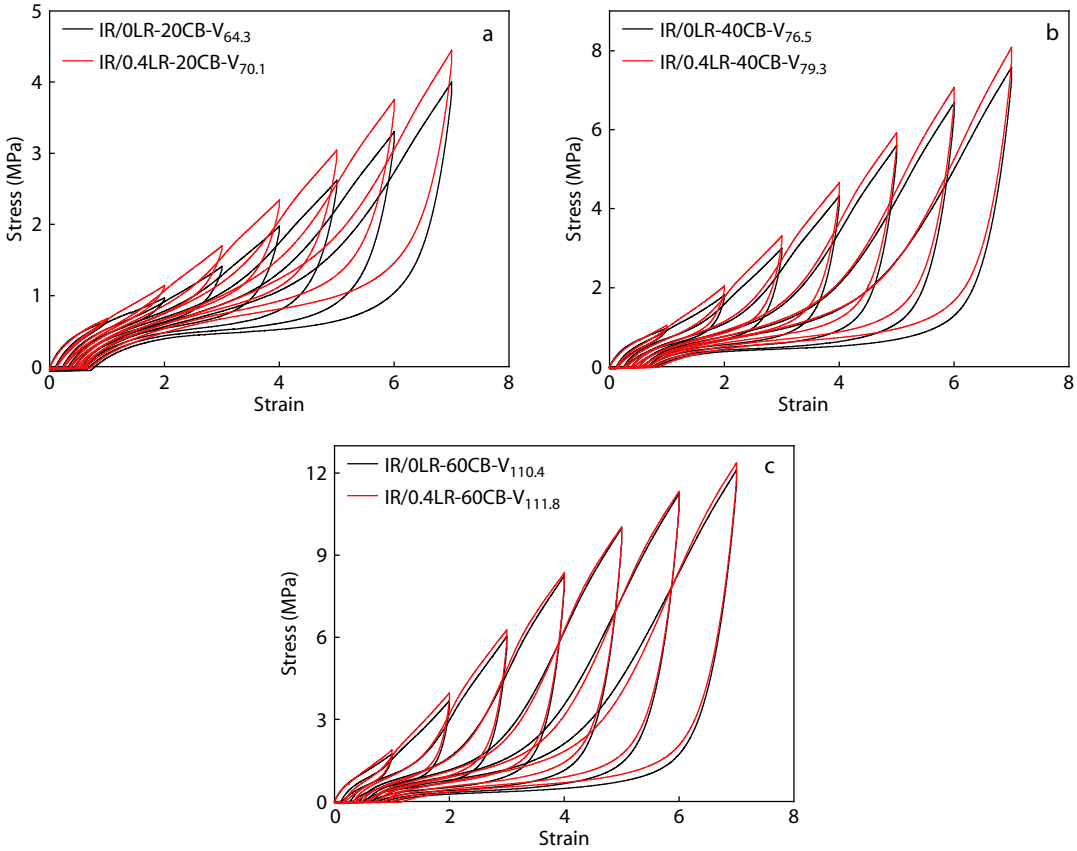

Fig. 9 Cyclic strain-stress relationships for IR/*i*LR-20CB-V_z (a), IR/*i*LR-40CB-V_z (b) and IR/*i*LR-60CB-V_z vulcanizates (c).

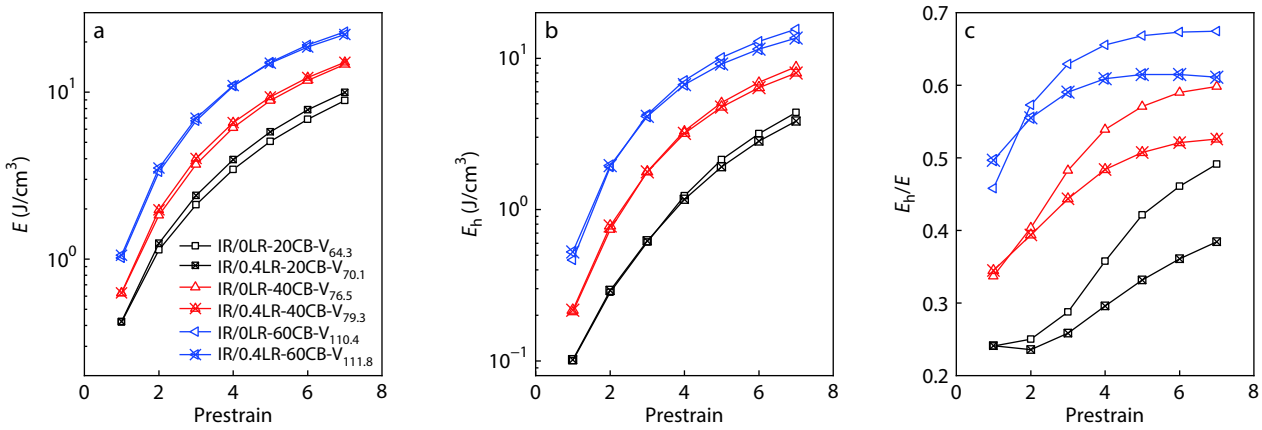

Fig. 10 Straining and hysteresis energies (E, a; E_h, b) and relative hysteresis energy (E_h/E, c) against prestrain.

investigated in detail in future.

CONCLUSIONS

It is a challenge to prepare rubber nanocomposites with high reinforcement efficiency and low energy dissipation. This long-standing issue is settled herein by using LR in CB filled IR vulcanizates. LR does not influence the filler-rubber interaction and the formations of glassy layer and bound rubber while it improves the ω-dependence of G'' and the critical strain amplitude of Payne effect. By changing ν_e and/or LR content, the Mullins effect can be tuned, and the accompanied mechanical hysteresis can be reduced without significant influence on the mechanical performances.

Electronic Supplementary Information

Electronic supplementary information (ESI) is available free of charge in the online version of this article at http://doi.org/10.1007/s10118-021-2550-y.

ACKNOWLEDGMENTS

This work was financially supported by the National Natural Science Foundation of China (Nos. U1908221, 51873190 and 51790503) and the Fundamental Research Funds for the Central Universities (No. 2020XZZX002-08).

REFERENCES

1 Guth, E. Theory of filler reinforcement. *J. Appl. Phys.* **1945**, *16*, 20–25.
2 Mooney, M. The viscosity of a concentrated suspension of spherical particles. *J. Colloid Sci.* **1951**, *6*, 162–170.
3 Krieger, I. M. Rheology of monodisperse latices. *Adv. Colloid Interface Sci.* **1972**, *3*, 111–136.
4 Schroyen, B.; Swan, J. W.; van Puyvelde, P.; Vermant, J. Quantifying the dispersion quality of partially aggregated colloidal dispersions by high frequency rheology. *Soft Matter* **2017**, *13*, 7897–7906.
5 Kraus, G. Mechanical losses in carbon-black-filled rubbers. *Appl. Polym. Symp.* **1984**, 75–92.
6 Zhu, Z.; Thompson, T.; Wang, S. Q.; Von Meerwall, E. D.; Halasa, A. Investigating linear and nonlinear viscoelastic behavior using model silica-particle-filled polybutadiene. *Macromolecules* **2005**, *38*, 8816–8824.
7 Lewicki, J. P.; Maxwell, R. S.; Patel, M.; Herberg, J. L.; Swain, A. C.; Liggat, J. J.; Pethrick, R. A. Effect of *meta*-carborane on segmental dynamics in a bimodal poly(dimethylsiloxane) network. *Macromolecules* **2008**, *41*, 9179–9186.
8 Song, Y.; Zheng, Q. Concepts and conflicts in nanoparticles reinforcement to polymers beyond hydrodynamics. *Prog. Mater. Sci.* **2016**, *84*, 1–58.
9 Payne, A. R.; Whittaker, R. E. Low strain dynamic properties of filled rubbers. *Rubber Chem. Technol.* **1971**, *44*, 440–478.
10 Payne, A. R.; Whittake, R. E. Effect of vulcanization on low-strain dynamic properties of filled rubbers. *J. Appl. Polym. Sci.* **1972**, *16*, 1191–1212.
11 Diani, J.; Fayolle, B.; Gilormini, P. A review on the Mullins effect. *Eur. Polym. J.* **2009**, *45*, 601–612.
12 Nagaraja, S. M.; Mujtaba, A.; Beiner, M. Quantification of different contributions to dissipation in elastomer nanoparticle composites. *Polymer* **2017**, *111*, 48–52.
13 Robertson, C. G.; Wang, X. Isoenergetic jamming transition in particle-filled systems. *Phys. Rev. Lett.* **2005**, *95*, 075703.
14 Zhao, D.; Ge, S.; Senses, E.; Akcora, P.; Jestin, J.; Kumar, S. K. Role of filler shape and connectivity on the viscoelastic behavior in polymer nanocomposites. *Macromolecules* **2015**, *48*, 5433–5438.
15 Cassagnau, P. Melt rheology of organoclay and fumed silica nanocomposites. *Polymer* **2008**, *49*, 2183.
16 Merabia, S.; Sotta, P.; Long, D. R. A microscopic model for the reinforcement and the nonlinear behavior of filled elastomers and thermoplastic elastomers (Payne and Mullins effects). *Macromolecules* **2008**, *41*, 8252–8266.
17 Majesté, J. C.; Vincent, F. A kinetic model for silica-filled rubber reinforcement. *J. Rheol.* **2015**, *59*, 405–427.
18 Sternstein, S. S.; Zhu, A. J. Reinforcement mechanism of nanofilled polymer melts as elucidated by nonlinear viscoelastic behavior. *Macromolecules* **2002**, *35*, 7262–7273.
19 Li, Z.; Xu, H.; Xia, X.; Song, Y.; Zheng, Q. Energy dissipation accompanying Mullins effect of nitrile butadiene rubber/carbon black nanocomposites. *Polymer* **2019**, *171*, 106–114.
20 Hou, F.; Song, Y.; Zheng, Q. Payne effect of thermo-oxidatively aged isoprene rubber vulcanizates. *Polymer* **2020**, *195*, 122432.
21 Xu, H.; Xia, X.; Hussain, M.; Song, Y.; Zheng, Q. Linear and nonlinear rheological behaviors of silica filled nitrile butadiene rubber. *Polymer* **2018**, *156*, 222–227.
22 Li, Z.; Wen, F.; Hussain, M.; Song, Y.; Zheng, Q. Scaling laws of Mullins effect in nitrile butadiene rubber nanocomposites. *Polymer* **2020**, *193*, 122350.
23 Acosta, R. H.; Monti, G. A.; Villar, M. A.; Valles, E. M.; Vega, D. A. Transiently trapped entanglements in model polymer networks. *Macromolecules* **2009**, *42*, 4674–4680.
24 Agudelo, D. C.; Roth, L. E.; Vega, D. A.; Valles, E. M.; Villar, M. A. Dynamic response of transiently trapped entanglements in polymer networks. *Polymer* **2014**, *55*, 1061–1069.
25 Chasse, W.; Lang, M.; Sommer, J. U.; Saalwachter, K. Cross-link density estimation of PDMS networks with precise consideration of networks defects. *Macromolecules* **2012**, *45*, 899–912.
26 Campise, F.; Roth, L. E.; Acosta, R. H.; Villiar, M. A.; Valles, E. M.; Monti, G. A.; Vega, D. A. Contribution of linear guest and structural pendant chains to relaxational dynamics in model polymer networks probed by time-domain ^{1}H NMR. *Macromolecules* **2016**, *49*, 387–394.
27 Batra, A.; Cohen, C.; Archer, L. Stress relaxation of end-linked polydimethylsiloxane elastomers with long pendent chains. *Macromolecules* **2005**, *38*, 7174–7180.
28 Vega, D. A.; Villar, M. A.; Alessandrini, J. L.; Valles, E. M. Terminal relaxation of model poly(dimethylsiloxane) networks with pendant chains. *Macromolecules* **2001**, *34*, 4591–4596.
29 Yamazaki, H.; Takeda, M.; Kohno, Y.; Ando, H.; Urayama, K.; Takigawa, T. Dynamic viscoelasticity of poly(butyl acrylate) elastomers containing dangling chains with controlled lengths. *Macromolecules* **2011**, *44*, 8829–8834.
30 Urayama, K.; Miki, T.; Takigawa, T.; Kobjiya, S. Damping elastomer based on model irregular networks of end-linked poly(dimethylsiloxane). *Chem. Mater.* **2004**, *16*, 173–178.
31 Li, Z.; Lu, X.; Tao, G.; Guo, J.; Jiang, H. Damping elastomer with broad temperature range based on irregular networks formed by end-linking of hydroxyl-terminated poly(dimethylsiloxane). *Polym. Eng. Sci.* **2016**, *56*, 97–102.
32 Yasuda, Y.; Minoda, S.; Ohashi, T.; Yokohama, H.; Ikeda, Y. Two-phase network formation in sulfur crosslinking reaction of isoprene rubber. *Macromol. Chem. Phys.* **2014**, *215*, 971–977.
33 Ikeda, Y.; Higashitani, N.; Hijikata, K.; Kokubo, Y.; Morita, Y.; Shibayama, M.; Osaka, N.; Suzuki, T.; Endo, H.; Kohjiya, S. Vulcanization: new focus on a traditional technology by small-angle neutron scattering. *Macromolecules* **2009**, *42*, 2741–2748.
34 Glebova, Y.; Reiter-Scherer, V.; Suvanto, S.; Korpela, T.; Pakkanen, T. T.; Severin, N.; Shershnev, V.; Rabe, J. P. Nano-mechanical imaging reveals heterogeneous cross-link distribution in sulfur-vulcanized butadiene-styrene rubber comprising ZnO particles. *Polymer* **2016**, *107*, 102–107.
35 Li, J.; Isayev, A. I.; Ren, X.; Soucek, M. D. Modified soybean oil-extended SBR compounds and vulcanizates filled with carbon black. *Polymer* **2015**, *60*, 144–156.
36 Betron, C.; Cassagnau, P.; Bounor-Legare, V. Control of diffusion and exudation of vegetable oils in EPDM copolymers. *Eur. Polym. J.* **2016**, *82*, 102–113.
37 Li, Z.; Ren, W.; Chen, H.; Ye, L.; Zhang, Y. Effect of liquid isoprene rubber on dynamic mechanical properties of emulsion polymerized styrene/butadiene rubber vulcanizates. *Polym. Int.* **2012**, *61*, 531–538.
38 Ren, Y.; Zhao, S.; Li, Q.; Zhang, X.; Zhang, L. Influence of liquid isoprene on rheological behavior and mechanical properties of polyisoprene rubber. *J. Appl. Polym. Sci.* **2015**, *132*, 41485.
39 Gruendken, M.; Velencoso, M. M.; Hirata, K.; Blume, A. Structure-propery relationship of low molecular weight 'liquid' polymers in blends of sulfur cured SSBR-rich compounds. *Polym. Test.* **2020**, *87*, 106558.
40 Horkay, F.; Mckenna, G. B.; Deschamps, P.; Geissler, E. Neutron

scattering properties of randomly cross-linked polyisoprene gels. *Macromolecules* **2000**, *33*, 5215–5220.
41 Senses, E.; Akcora, P. Tuning mechanical properties of nanocomposites with bimodal polymer bound layers. *RSC Adv.* **2014**, *4*, 49628–49634.
42 Liu, J.; Wu, Y.; Shen, J.; Gao, Y.; Zhang, L.; Cao, D. Polymer-nanoparticle interfacial behavior revisited: a molecular dynamics study. *Phys. Chem. Chem. Phys.* **2011**, *13*, 13058–13069.
43 Karatrantos, A.; Clarke, N. A theoretical model for the prediction of diffusion in polymer/SWCNT nanocomposites. *Soft Matter* **2011**, *7*, 7334–7341.
44 Zheng, X.; Sauer, B. B.; Vanalsten, J. G.; Schwarz, S. A.; Rafailovich, M. H.; Sokolov, J.; Rubinstein, M. Reptation dynamics of a polymer melt near an attractive solid interface. *Phys. Rev. Lett.* **1995**, *74*, 407–410.
45 Baeza, G. P.; Dalmas, F.; Dutertre, F.; Majeste, J. C. Isostructural softening of vulcanized nanocomposites. *Soft Matter* **2020**, *16*, 3180–3186.
46 Trinh, G. H.; Desloir, M.; Dutertre, F.; Majeste, J. C.; Dalmas, F.; Baeza, G. P. Isostructural softening of the filler network in SBR/silica nanocomposites. *Soft Matter* **2019**, *15*, 3122–3132.
47 Zhang, Q.; Xu, H.; Song, Y.; Zheng, Q. Influence of hydroxyl-terminated polybutadiene liquid on rheology of fumed silica filled *cis*-polybutadiene rubber. *Polymer* **2019**, *180*, 121709.
48 Xu, H.; Ding, L.; Song, Y.; Wang, W. Rheology of end-linking polydimethylsiloxane networks filled with silica. *J. Rheol.* **2020**, *64*, 1425–1438.
49 Subbotin, A.; Semenov, A.; Hadziioannou, G.; ten Brinke, G. Nonlinear rheology of confined polymer melts under oscillatory flow. *Macromolecules* **1996**, *29*, 1296–1304.
50 Sarvestani, A. S. Nonlinear rheology of unentangled polymer melts reinforced with high concentration of rigid nanoparticles. *Nanoscale Res. Lett.* **2010**, *5*, 791–794.
51 Fu, W.; Wang, L.; Huang, J.; Liu, C.; Peng, W.; Xiao, H.; Li, S. Mechanical properties and Mullins effect in natural rubber reinforced by grafted carbon black. *Adv. Polym. Tech.* **2019**, *2019*, 4523696.
52 Sodhani, D.; Reese, S. Finite element-based micromechanical modeling of microstructure morphology in filler-reinforced elastomer. *Macromolecules* **2014**, *47*, 3161–3169.
53 Stöckelhuber, K. W.; Svistkov, A. S.; Pelevin, A. G.; Heinrich, G. Impact of filler surface modification on large scale mechanics of styrene butadiene/silica rubber composites. *Macromolecules* **2011**, *44*, 4366–4381.
54 Yatsuyanagi, F.; Suzuki, N.; Ito, M.; Kaidou, H. Effects of secondary structure of fillers on the mechanical properties of silica filled rubber systems. *Polymer* **2001**, *42*, 9523–9529.
55 Bhattacharyya, S.; Sinturel, C.; Bahloul, O.; Saboungi, M. L.; Thomas, S.; Salvetat, J. P. Improving reinforcement of natural rubber by networking of activated carbon nanotubes. *Carbon* **2008**, *46*, 1037–1045.
56 Meissner, B.; Matějka, L. A structure-based constitutive equation for filler-reinforced rubber-like networks and for the description of the Mullins effect. *Polymer* **2006**, *47*, 7997–8012.

https://doi.org/10.1007/s10118-021-2550-y